Journal of The Electrochemical Society, **159** (7) F249-F254 (2012)
0013-4651/2012/159(7)/F249/6/$28.00 © The Electrochemical Society

Facilitated Electro-Oxidation of Formic Acid at Nickel Oxide Nanoparticles Modified Electrodes

Gumaa A. El-Nagar,[a] Ahmad M. Mohammad,[a,b] Mohamed S. El-Deab,[a] and Bahgat E. El-Anadouli[a,z]

[a]*Department of Chemistry, Faculty of Science, Cairo University, Cairo, Egypt*
[b]*Department of Chemical Engineering, Faculty of Engineering, The British University in Egypt, Cairo, Egypt*

This study addresses the electrocatalytic oxidation of formic acid (FA) at nickel oxide nanoparticles (nano-NiO*x*) modified Pt, Au, GC anodes. FA oxidation proceeds at the unmodified Pt electrode with the appearance of two oxidation peaks at 0.25 and 0.65 V corresponding to the direct oxidation of FA to CO_2 and the oxidation of the poisoning intermediate, CO, to CO_2 with a current ratio of the two peaks less than 0.2. Interestingly, this ratio jumps up to more than 50, upon modifying Pt with nano-NiO*x*. This highlights the essential role of NiO*x* in enhancing the direct oxidation of FA (at 0.25 V) at Pt substrate. On the other hand, unmodified GC and Au anodes as well as those modified with nano-NiO*x* exhibit no catalytic response toward FA oxidation. This highlights the essential role of the underlying substrate and depicts also that nano-NiO*x* behaves as a catalytic mediator which facilitates the charge transfer during the oxidation of FA at Pt anode. Optimization of the surface coverage of nano-NiO*x* at Pt is achieved, aiming at maximizing the rate of the direct oxidation pathway of FA while suppressing the indirect oxidation route producing the poisoning CO. Moreover, nano-NiO*x*/Pt anode maintains its high catalytic activity for a prolonged time of continuous oxidation of FA.
 [DOI: 10.1149/2.043207jes]

Manuscript submitted February 10, 2012; revised manuscript received April 3, 2012. Published July 17, 2012.

Fuel cells represent a unique entry into the field of clean, noiseless, eco-friendly and efficient energy sources. They are expected to replace the fossil fuel-based energy sources to meet the growing unlimited needs of electric power in industry and daily live activities. Of these, the direct formic acid fuel cell (DFAFC) is a promising candidate, in view of its higher theoretical open-circuit potential (1.40 V) than that of the direct methanol fuel cells, DMFCs, (1.21 V). Moreover, FA (as a fuel) has a smaller crossover flux through Nafion membrane than methanol, which permits using a higher concentration of the fuel and thinner membranes. Platinum is considered among the best electrocatalysts for FA oxidation. However, its catalytic activity deteriorates with time due to the accumulation of the poisoning CO intermediate produced as a result of the "*non-faradaic*" dissociation of FA. This, eventually, blocks the active sites of Pt and lowers the kinetics of FA electro-oxidation. The search for efficient and catalytically active anodes for FA oxidation is the incentive behind several investigations. Most of these investigations have targeted the CO poisoning of the Pt-based electrodes in a way to reduce the amount of adsorbed CO or to facilitate its oxidative removal away from the electrode surface at low anodic potential. Interestingly, Pt-based alloys and composites,[1–7] and modified Rh, Pd and Au electrodes[8–10] have been suggested as possible anodes for FA oxidation which could successfully shift the reaction pathway toward the direct oxidation of FA to CO_2.[11–18]

In fact, the mechanism of FA oxidation at Pt-based electrodes adapts a dual-pathway.[6,19,20] The first involves the dehydrogenation of FA to CO_2, with the formation of formate anion as the reactive intermediate.[17,19,21] The second path involves the generation and adsorption of the dehydration product of FA (i.e., CO) at low potential domain and its oxidation to CO_2 at higher anodic potentials compared to the direct oxidation. The generation of CO accounts for the degradation of the catalytic activity of Pt with time.

The current study is concerned with the investigation of the electro-oxidation of FA at Pt, Au, and GC anodes modified with nano-NiO*x*, aiming at increasing the life time of the Pt catalyst by imparting a marked tolerance against CO poisoning to enhance the fuel cell efficiency. Fortunately, the modification of Pt with minute amounts of nano-NiO*x* results in a significant enhancement of the direct oxidation pathway of FA to CO_2 with a concurrent depression of the indirect pathway as well as a significant long term stability. This enhancement was not observed at the nano-NiO*x* modified GC and Au electrodes. The influence of the loading level of nano-NiO*x* on the catalytic activity of the modified Pt anodes is addressed herein as well.

Experimental

Electrodes.— Glassy carbon (d = 3.0 mm), polycrystalline Au (d = 1.6 mm) and polycrystalline Pt (d = 1.6 mm) electrodes served as the working electrodes. An Ag/AgCl/KCl (sat) and a spiral Pt wire were used as reference and counter electrodes, respectively. Conventional procedure was applied to clean the Pt, Au and GC electrodes as described elsewhere.[6,20,22]

Preparation of the modified electrodes.— The electrode's modification with nano-NiO*x* was achieved in two sequential steps. The first involved the electrodeposition of metallic nickel on the working electrode (i.e., Au, Pt and GC) from an aqueous solution of 0.1 M acetate buffer solution (ABS, pH = 4.0) containing 1 mM $Ni(NO_3)_2$ by a constant potential electrolysis at −1V vs. Ag/AgCl/KCl (sat.) for various durations. These durations were set to control the amount of the electrodeposited Ni. On the second step, the metallic Ni was passivated (oxidized) in 0.1 M phosphate buffer solution (PBS, pH = 7) by cycling the potential between −0.5 and 1 V vs. Ag/AgCl/KCl(sat) for 10 cycles at 200 mV/s.[23,24] It is worth to mention that, the surface coverage (θ) of the thus-fabricated nano-NiO*x* on the Pt electrode depends inherently on the time employed during the electrodeposition step. The values of θ are listed in Table I for various deposition times.

Table I. Variation of surface coverage (θ) of the nano-NiO*x* electrodeposited onto Pt electrode with deposition time.

Dep. time of nano-NiO*x*/s	Real surface area(S)[a]/cm^2 NiO*x*/Pt	Surface Coverage[b] (θ %)
0	0.096	0
30	0.092	4
60	0.067	20
90	0.059	40
120	0.038	60
150	0.038	62
180	0.021	76
240	0.023	78
360	0.008	92

[a]As estimated from the charge consumed during the reduction of the surface oxide monolayer (at ca. 0.5 V, Figure 5B) using a reported value of 420 μC cm^{-2}.[6,22]
[b]The values of surface coverage ($\theta = 1 - S_{modified}/S_{unmodified}$) were calculated for the various nano-NiO*x*/Pt electrodes. $S_{modified}$ and $S_{unmodified}$ refer to the real surface area of the modified and the unmodified Pt electrodes, respectively.

[z]E-mail: bahgat30@yahoo.com

The real surface areas of the unmodified (A_{bare}) and nano-NiO*x* modified (A_{mod}) Pt electrodes were estimated from the charge associated with the reduction of the surface Pt-oxide monolayer (cf Fig. 5) at ca. 500 mV in 0.5 M H_2SO_4 and at ca. −250 mV in 0.5 M KOH using a reported value of 420 μC/cm^2[6,22] and the corresponding values are shown in Table I.

Measurements.— The electrocatalytic activity of the nano-NiO*x* modified electrodes toward FA oxidation was examined in an aqueous solution of 0.3 M formic acid (pH = 3.5). The pH was adjusted by adding a proper amount of NaOH. As, the use of highly acidic solutions would diminish the stability of nickel oxide (albeit at slow kinetics), the current study is conducted at slightly acidic pH, which lies within the stability domain of nickel oxide.[25] Moreover, at this pH an appreciable amount of FA is ionized to formate anion (about one third). This would enhance the ionic conductivity in the solution, thus reduces the resistance polarization, in addition to compressing the thickness of the diffusion layer.

Cyclic voltammetry (CV) was performed in a conventional two-compartment three-electrode glass cell. All measurements were performed at room temperature (25 ± 1°C) using an EG&G potentiostat (model 273A) operated with Echem 270 software. A field emission scanning electron microscope, FE-SEM, (QUANTA FEG 250) coupled with an energy dispersive X-ray spectrometer (EDS) unit was employed to evaluate the electrode's morphology and surface composition. X-ray diffraction, XRD, (PANalytical, X'Pert PRO) operated with Cu target (λ = 1.54Å) was used to identify the crystallographic structure of the nano-NiO*x*. Current densities were calculated on the basis of the real surface area of the working electrodes.

Results and Discussion

Electrochemical and morphological characterization.— Fig. 1A-1C compares the CVs of the unmodified (solid lines) and the nano-NiO*x* modified (dashed lines) (A) Pt, (B) Au, and (C) GC electrodes in 0.5 M KOH. Fig. 1A (solid line) depicts clearly a typical characteristic CV of a clean polycrystalline Pt electrode in 0.5 M KOH.[26] Interestingly, upon modifying the bare Pt electrode with nano-NiO*x* (Fig. 1A, dashed line) a noticeable decrease in the intensity of the reduction peak of the Pt oxide (at ca. −0.26 V) is observed along with a decrease in the current of the hydrogen adsorption/desorption peaks (in the potential region from −0.6 to–0.9 V vs. Ag/AgCl/KCl (sat)). Moreover, a redox couple is observed, at ca. 0.4 V, which corresponds to the $Ni(OH)_2$/NiOOH transformation.[27] Similar redox responses for the Ni(II)/Ni(III) transformation are obtained at nano-NiO*x* modified Au and GC electrodes, respectively shown in Fig. 1B and 1C. The surface coverage (θ) was estimated as 76% and 70% for the nano-NiO*x* modified Pt and Au electrodes, respectively. This reveals the partial coverage of the underlying substrates with nano-NiO*x*.

The morphological characterization of the modified electrodes is disclosed by SEM imaging. Fig. 2 shows typical SEM micrographs of nickel before (A) and after passivation (B). It reveals that the electrodeposited Ni has a dendritic nanostructure with an average particle size of 80 nm that partially covers the surface of GC electrode (image A). Similar morphology is observed after passivation, with a larger average particle size (150 nm, see image B).

Fig. 3 shows XRD patterns of NiO*x* fabricated at (A) GC, (B) Au and (C) Pt substrates. In Fig. 3A, the signals observed at 2 Theta equal to 25.2, 37.9 and 43.1° are assigned to the NiOOH phase (PDF card 00-006-0075). The other peaks located at 2 Theta of 62.2 and 78.6° are assigned to lower Ni-Oxide phase (PDF card 01-071-4750).[28]

Fig. 3B and 3C shows similar diffraction patterns of the NiOOH phase (at 2 Theta of 37.9 and 42.8°) along with the diffraction signals of polycrystalline Au and Pt substrates, respectively.

Effect of substrate.— The catalytic activity of nanoparticle-based electrodes is shown to depend markedly on several factor including the nature of the substrate.[6,29] In this context, the electrocatalytic

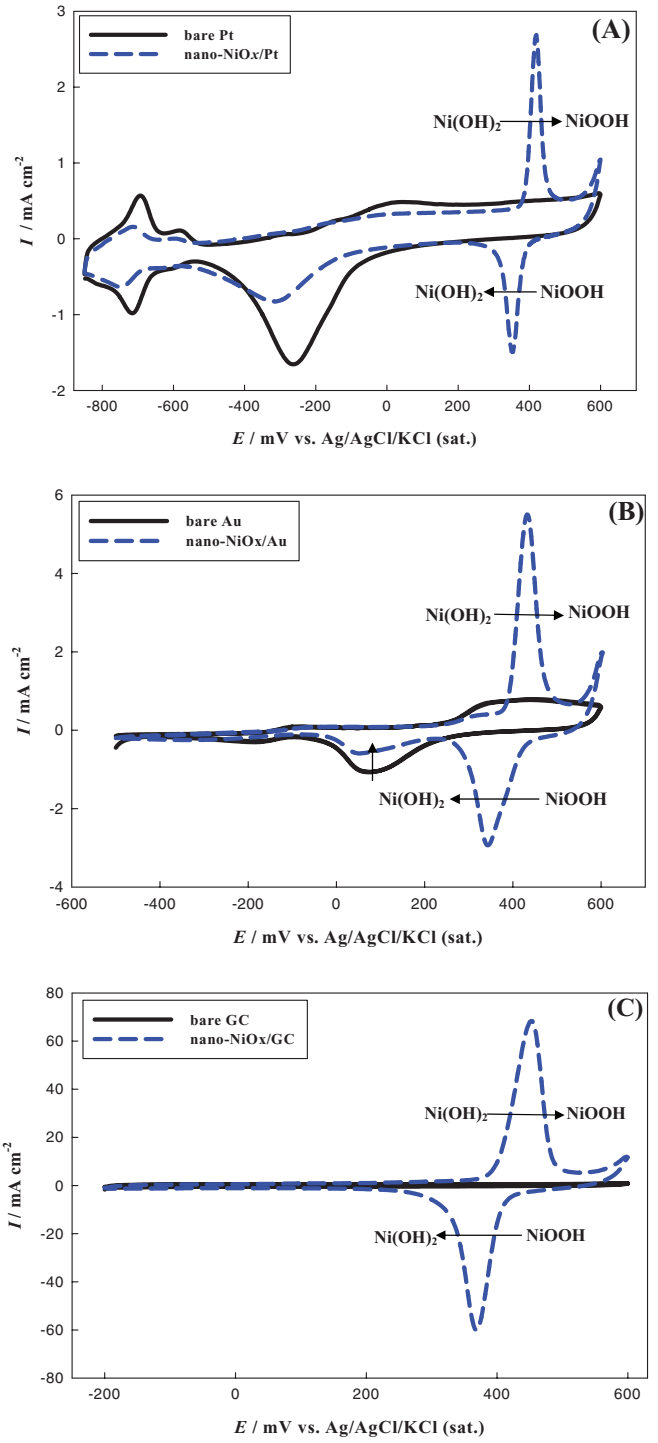

Figure 1. (A-C) CVs of unmodified and nano-NiO*x* modified (A) Pt, (B) Au and (C) GC electrodes in 0.5M KOH solution at 100 mV s^{-1}. Note that nano-NiO*x* was electrodeposited onto the various electrodes as described in the Experimental section using a deposition time of 3 min.

activity of nano-NiO*x* toward FA oxidation is investigated at three different (nano-NiO*x* modified GC, Au and Pt) electrodes and the corresponding CVs are shown in Fig. 4. In Fig. 4A (solid line), two oxidation peaks (marked as I_p^d and I_p^{ind}) were observed at ca. 0.25 and 0.6 V in the forward direction (i.e., anodic-going potential scan) at unmodified Pt electrode, similar to previous reports.[6,20,30] The first peak (I_p^d), located at ca. 0.25 V, is assigned to the direct oxidation of FA (i.e., dehydrogenation pathway) to CO_2. Whereas, the second

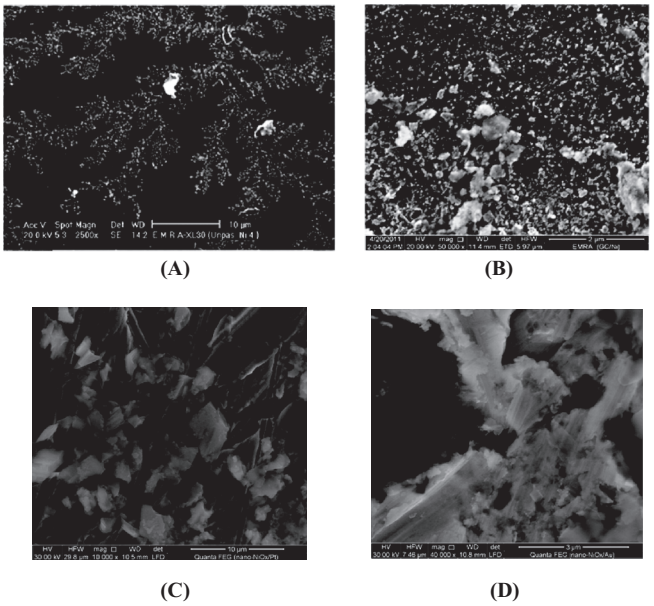

Figure 2. FE-SEM images of (A) metallic nickel and (B-D) nano-NiO*x* modified (A,B) GC and (C) Pt and (D) Au electrodes. N.B. Ni metal was electrodeposited as described in the experimental section by a constant potential electrolysis at −1V vs. Ag/AgCl/KCl (sat.) for 3 min. Scale bar = 10 μm for images A and C, = 2 μm for image B and = 3 μm for image D.

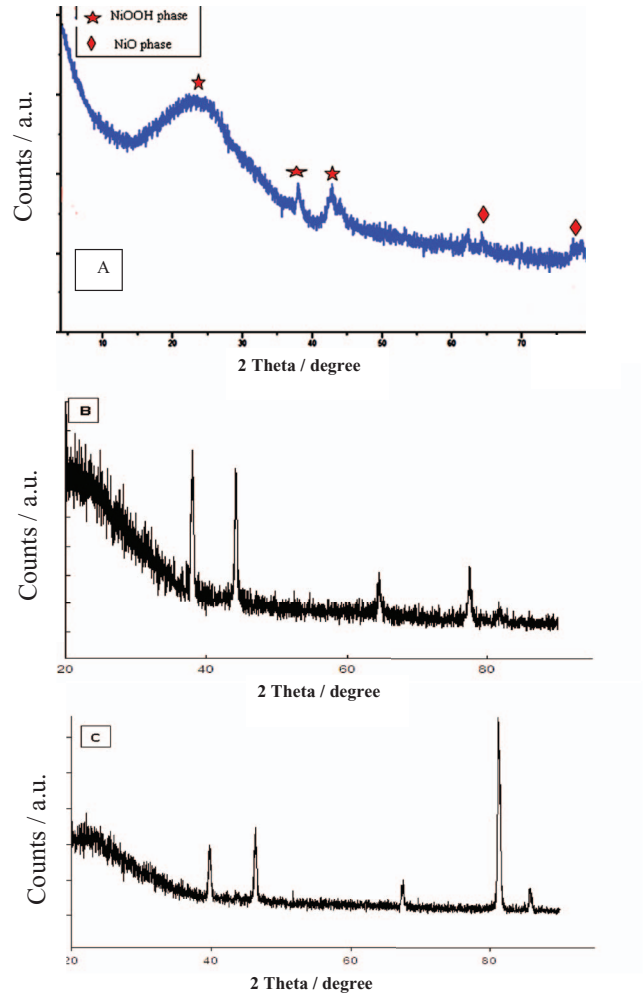

Figure 3. XRD pattern for the fabricated NiO*x* at (A) GC, (B) Au and (C) Pt substrates.

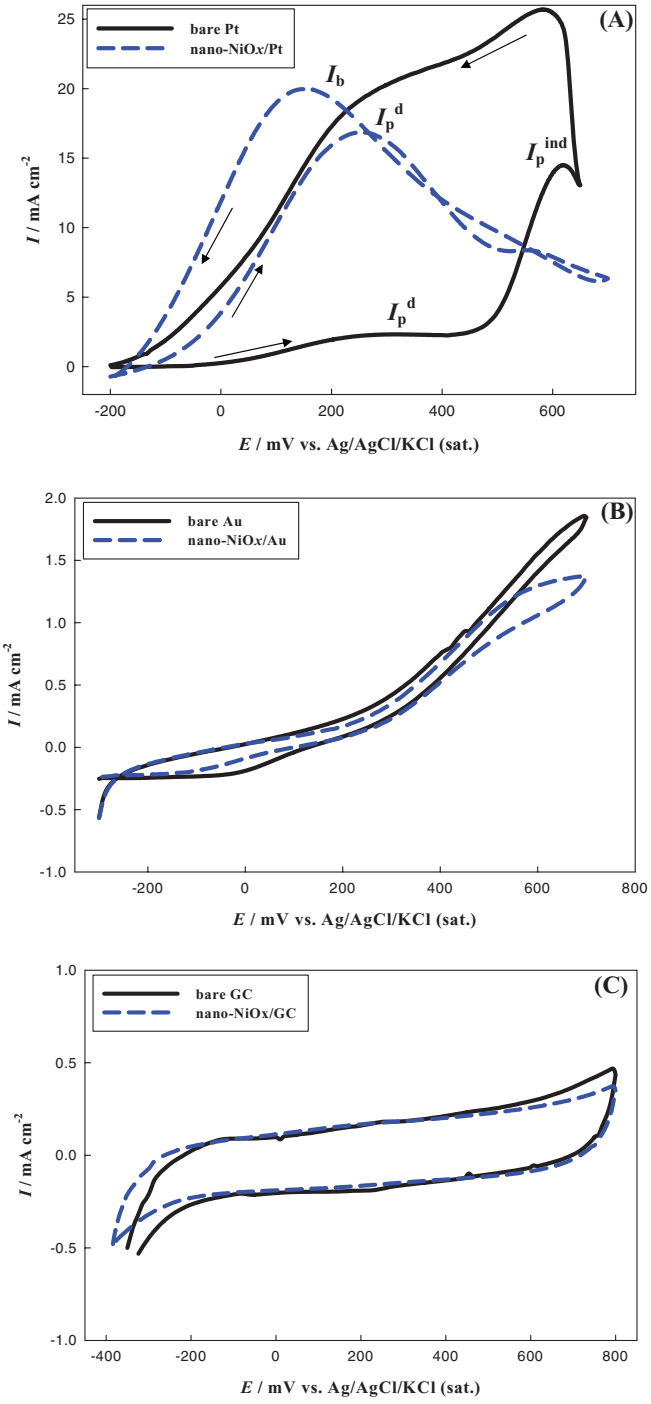

Figure 4. CVs for formic acid oxidation at unmodified (solid lines) and nano-NiO*x* modified (dashed lines) (A) Pt, (B) Au and (C) GC electrodes in 0.3 M HCOOH solution (pH 3.5) measured at 100 mV s^{-1}.

oxidation peak (at ca. 0.6 V) corresponding to the oxidation of the adsorbed CO to CO_2 commences. Upon modifying the Pt electrode with nano-NiO*x* (Fig. 4A, dashed line), a significant increase in the first peak intensity, I_p^d, is observed concurrently with a noticeable depression of the second oxidation peak intensity, I_p^{ind}. The depression of the indirect oxidation peak, I_p^{ind}, means that less CO are formed at the modified surface, i.e., the presence of nano-NiO*x* seems to retard the *non-faradaic* dissociation of FA. Alternatively, it can be the catalytic role of nano-NiO*x* that facilitates the CO oxidation at a lower potential.[31,32] The ratio of the two oxidation peaks (I_p^d and I_p^{ind}) reflects the preferential oxidation pathway of FA at a particular

electrode. The ratio between the two oxidation peaks, I_p^d/I_p^{ind} is ca. 0.2 at unmodified Pt and jumps up to ca. 50 at nano-NiO*x* modified Pt electrode (i.e., about 250 times higher). This enhancement is also manifested if one considers the increase of the charge consumed during the direct oxidation of FA at the unmodified and nano-NiOx modified Pt electrodes, which amounts to 10.6 and 67.5 mC cm^{-2}, respectively, i.e., by ca. 6 times. Interestingly this oxidation charge (67.5 mC cm^{-2}) is higher than the sum of charges consumed for the direct (10.6 mC cm^{-2}) and indirect oxidation (26.1 mC cm^{-2}) pathways of FA at the unmodified Pt electrode. This fact reflects three points:

(i) The oxidation of FA is shifted towards the direct pathway at the modified electrode,
(ii) The nano-NiO*x*/Pt electrode (albeit with a lower accessible surface area of Pt) oxidizes more FA molecules, i.e., it has a higher activity compared to the unmodified Pt, (N.B. the surface coverage issue is discussed below), and
(iii) Moreover, the direct oxidation of one FA molecule to CO_2 (requires two electrons) proceeds at a higher rate at the modified Pt electrode than the oxidation of CO to CO_2 (requires two electrons) at the unmodified Pt electrode.

Another catalytic probe is given by the I_p^d/I_b ratio (I_b is the oxidation peak current intensity measured during the reverse (cathodic-going) potential scan. That is a low I_p^d/I_b ratio indicates poor oxidation of FA to CO_2 - during the forward potential scan - and accumulation of incompletely oxidized carbonaceous species (e.g., CO) at the electrode surface prevails. In the present case, a value of I_p^d/I_b close to unity is obtained at nano-NiO*x*/Pt (Fig. 4A, dashed line), which is much higher than that observed at the unmodified Pt (Fig. 4A, solid line). Both measurements indicate the high electrocatalytic activity of the modified electrode toward FA oxidation in the cathodic as well as the anodic potential scan directions.

On the other hand, the unmodified and nano-NiO*x* modified Au (Fig. 4B) and GC (Fig. 4C) electrodes did not show any significant catalytic response toward FA oxidation. This obviously depicts that FA oxidation is a substrate dependent reaction, and it further highlights the importance of the chemisorption step of FA at the substrate as a prerequisite for its subsequent oxidation.[19,21,33] This chemisorption step is feasible at Pt substrates due to the favorable heat of adsorption of FA at Pt surface compared with Au and GC substrates.[34] However, Pt (albeit a crucial component) does not support the direct oxidation of FA at a reasonable rate. Thus, nano-NiO*x* is believed to act as a catalytic mediator (possibly through a reversible Ni(II)/Ni(III) redox system, see Eq. (1) below) which facilitates the charge transfer during the direct oxidation of FA to CO_2 (see Eq. (2)). On parallel, nano-NiO*x* might facilitate the oxidation of the poisoning CO intermediate at a reasonably low potential (see Eq. (3)). Recent reports provided arguments supporting the catalytic enhancement of CO oxidation (to CO_2) by manganese oxide nanostructures in similar media.[32]

In this context, the following set of equations is proposed as a plausible explanation of the observed enhancing role of nano-NiO*x* through a reversible transformation between lower (II) and higher (III) oxidation states of Ni oxides as follows:

$$Ni(OH)_2 \leftrightarrow NiOOH + H^+ + e^- \quad (1)$$

Thermodynamically, the above reaction is feasible under the prevailing conditions of pH and potential. The electrogenerated NiOOH species react with FA (and formate anions) as follows:

$$Pt\ldots HCOOH_{ads} + NiOOH \rightarrow Pt_{free} + CO_2 + Ni(OH)_2 + H^+ + e^- \quad (2a)$$

$$Pt\ldots HCOO^-_{ads} + NiOOH \rightarrow Pt_{free} + CO_2 + Ni(OH)_2 + e^- \quad (2b)$$

and/or

$$Pt\ldots CO_{ads} + NiOOH + H_2O \rightarrow Pt_{free} + Ni(OH)_2 + CO_2 + H^+ + e^- \quad (3)$$

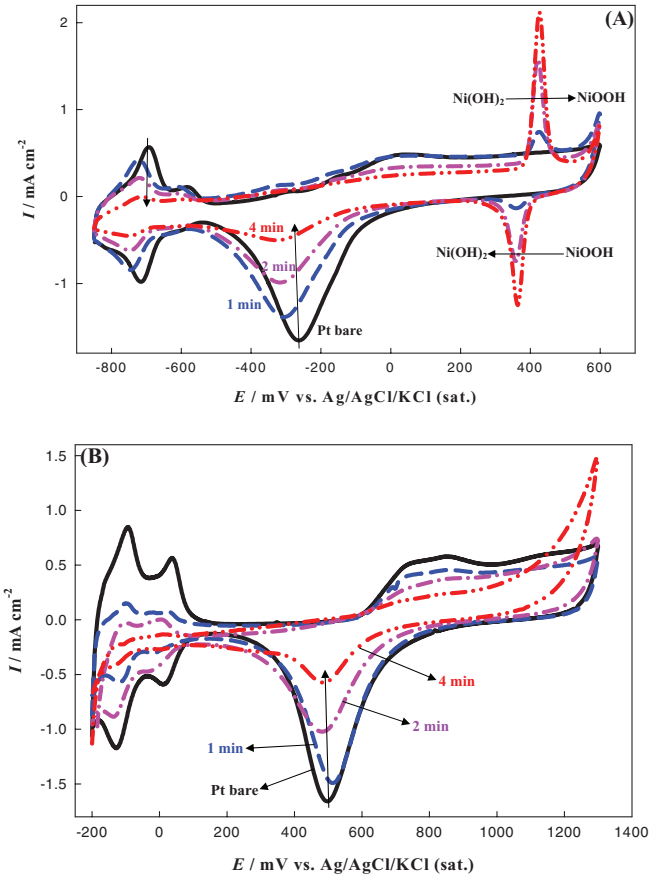

Figure 5. (A) CVs obtained in 0.5 M KOH at the unmodified (solid black line) and nano-NiO*x* modified Pt (broken lines) electrodes with various loading levels of the nano-NiO*x* (deposition time: 1, 2, and 4 min) at 100 mV s^{-1}. (B) CVs obtained in 0.5 M H_2SO_4 at the unmodified (solid black line) and nano-NiO*x* modified Pt (broken lines) electrodes with various loading levels of the nano-NiO*x* (deposition time: 1, 2, and 4 min) at 100 mV s^{-1}.

Addition of Eq. (1) to (2a) and (2b) gives:

$$Pt\ldots HCOOH_{ads} \rightarrow Pt_{free} + CO_2 + 2H^+ + 2e^- \quad (4a)$$

$$Pt\ldots HCOO^-_{ads} \rightarrow Pt_{free} + CO_2 + H^+ + 2e^- \quad (4b)$$

Also, addition of Eq. (1) and Eq. (3) gives:

$$Pt\ldots CO_{ads} + H_2O \rightarrow Pt_{free} + CO_2 + 2H^+ + 2e^- \quad (5)$$

Eq. (4a) and (4b) displays that the observed oxidation current is solely supported by the oxidation of FA, and nickel oxide functions as a catalytic mediator. Moreover, Reactions 2 and 3 indicate the regeneration of $Ni(OH)_2$[27] which is believed to start new cycles of catalytic mediation through the above set of equations. In all cases, NiOOH helps the retrieval of Pt active sites for the further oxidation to proceed.

Effect of nano-NiOx loading level.— Optimization of the loading level of nano-NiO*x* (i.e., surface coverage) onto Pt electrode toward the electrocatalytic oxidation of FA has been investigated. Several sets of CVs are measured. Fig. 5A and 5B shows the characteristic CVs obtained at the nano-NiO*x* modified Pt electrode with different loading levels of the nano-NiO*x* measured in alkaline and acidic media, respectively. This figure shows a gradual decrease of the intensity of the reduction peak of Pt oxide and the hydrogen adsorption/desorption peaks with the loading of nano-NiO*x*. On parallel, it depicts a systematic increase in the intensity of the redox peak couple at ca. 400 mV, which corresponds to $Ni(OH)_2$/NiOOH surface transformation.[23,35–37]

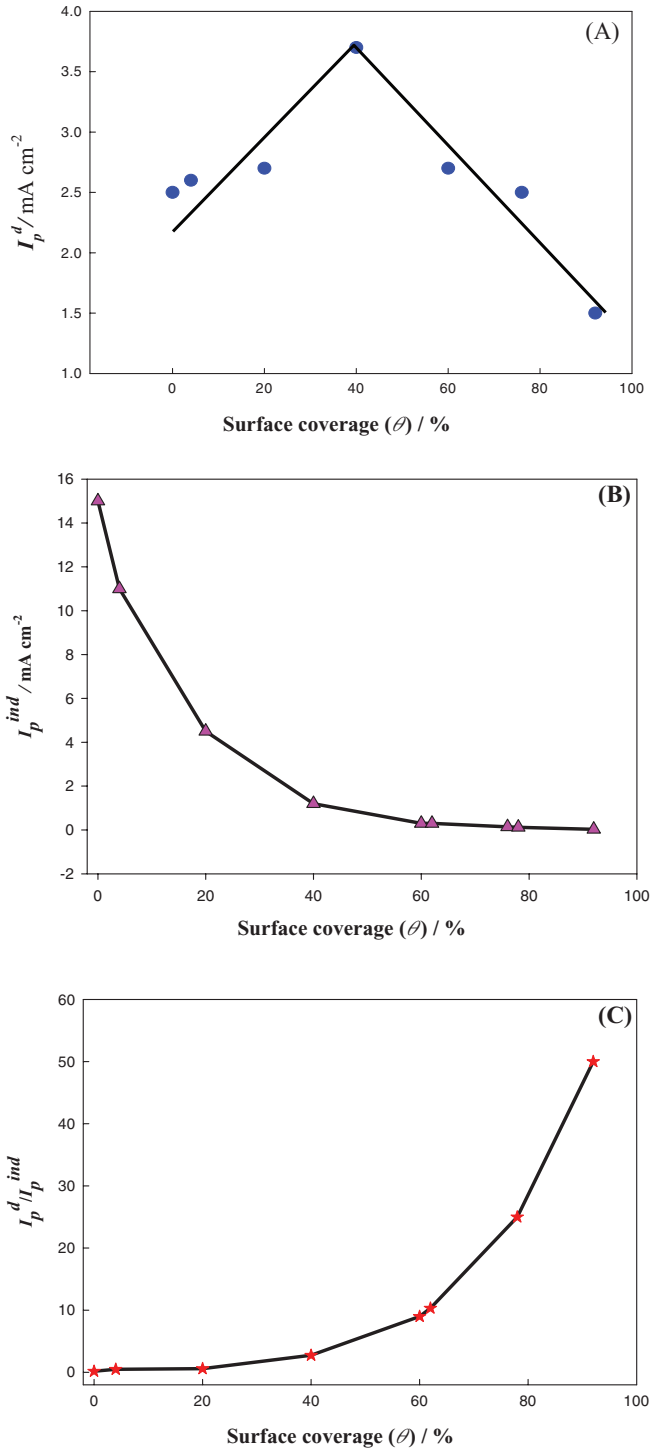

Figure 6. The variation of (A) I_p^d, (B) I_p^{ind} and (C) I_p^d / I_p^{ind} with surface coverage (θ) of nano-NiO*x* onto Pt electrode.

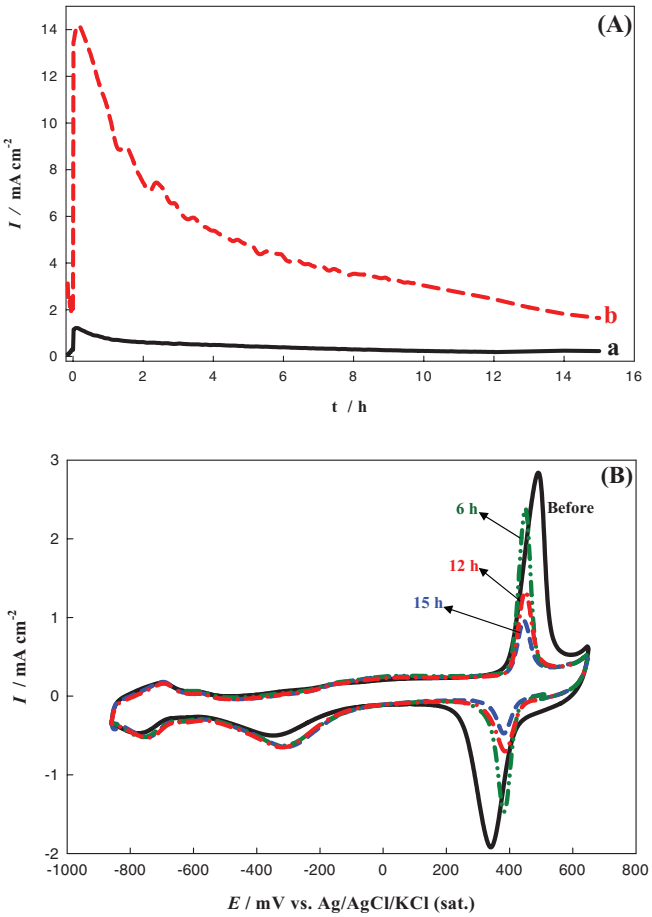

Figure 7. (A) the current transients obtained during formic acid oxidation at (a) Pt and (b) nano-NiO*x*/Pt in 0.3 M HCOOH (pH 3.5) at a potential of +300 mV vs. Ag/AgCl/KCl (sat.). (B) CVs response obtained nano-NiO*x* / Pt before (solid line-black) and (b) after aging (dashing lines) for 6, 12 and 15 hours in HCOOH solution with pH 3.5 at + 300 mV in 0.5 M KOH with scan rate 100 mV s^{-1}.

Figure 5 indicates the successful and feasible control of nano-NiO*x* surface coverage on Pt substrate.

Fig. 6A-6C shows the variation of the oxidation peak currents (I_p^d and I_p^{ind}) and ratio between the two oxidation peaks (I_p^d / I_p^{ind}) of FA with surface coverage (θ) of nano-NiO*x*. The direct peak current, I_p^d, increased up to a certain limit with θ and then decreased (Fig. 6A). This makes sense as the catalytic activity of the nano-NiO*x*/Pt electrode is expected to increase with the loading of the catalytic mediator, as long as the accessible surface area of Pt is sufficient. Beyond certain coverage, the decrease in the accessible surface area of Pt becomes a controlling factor in the rate of direct oxidation process. Concurrently, a monotonic decrease of the indirect peak current I_p^{ind}, with θ is observed (Fig. 6B). In other words, the increase of the loading level of the catalytic mediator (i.e., nano-NiO*x*) decreases the possibility of the indirect oxidation of FA by decreasing the amount of CO generated at the surface and/or facilitating its oxidation at such a low potential similar to that observed for the direct oxidation of FA to CO_2.

Interestingly, Fig. 6C shows that the ratio I_p^d/ I_p^{ind} always increases with θ, over the whole range of surface coverage. This indicates that the decrease of I_p^{ind} is much faster than the increase of I_p^d, beyond the optimum θ value. Again this emphasizes the catalytic enhancing role of nano-NiO*x* in favoring the FA direct oxidation.

Stability of nano-NiOx/Pt electrode.— The stability of the proposed catalyst has been investigated by chronoamperometry at a potential of 300 mV vs. Ag/AgCl/KCl (sat.) which is close to the anodic peak potential of direct FA oxidation. Fig. 7 depicts that the current density of FA oxidation at nano-NiO*x*/Pt electrode is by 11 times higher than that observed at the unmodified electrode, at early stage of electrolysis. After a prolonged electrolysis time up to 6 h, the oxidation currents amount to ca. 4 mA cm^{-2} at nano-NiO*x*/Pt electrode which is by 8 times larger that that measured at the unmodified Pt electrode (0.5 mA cm^{-2}). Moreover, the decay in oxidation of FA is higher at bare Pt than that observed at nano-NiO*x*/Pt electrode. This demonstrates a noticeable stability as well as a high CO tolerance of

nano-NiO*x*/Pt electrode. However, a partial dissolution and/or deactivation of nano-NiO*x* may account for the observed decay in current at the nano-NiO*x*/Pt electrode. This urged us to probe the catalytic redox response of the nano-NiOx/Pt electrode after a prolonged time of electrolysis.

Fig. 7B shows CVs for the nano-NiO*x*/Pt (used in Fig. 6) measured in 0.5 M KOH before (solid black line) and after a prolonged oxidation of FA for 6, 12 and 15 h (dashed colored lines). This figure depicts insignificant change in the surface coverage of nano-NiO*x* at Pt substrate after the prolonged electrolysis of FA. This reflects a good mechanical stability and good adhesion of nano-NiO*x* on the Pt electrode. However, a significant decrease, albeit to different extents, in the current intensities of the redox couples was observed corresponding to the $Ni(OH)_2$/NiOOH transformation. This decrease in the peak currents of the $Ni(OH)_2$/NiOOH redox can reasonably account for the observed gradual decay of FA oxidation current. It may arise from the reversion of the active β-NiOOH phase to an inactive phase of Ni oxide (γ-NiOOH)[38] at the surface as a result of the excessive oxidation of FA.

Conclusions

A novel nano-NiO*x* modified Pt catalyst for the direct electrooxidation of formic acid (FA) was developed. This modification resulted in a superb enhancement of the direct oxidation pathway of formic acid to CO_2. The ratio I_p^d/I_p^{ind} increased about 250 times upon modifying the Pt substrate with a minute amount of nano-NiO*x*. This reflects that the direct dehydrogenation pathway has become preferential for the FA oxidation. The ratio between the two oxidation peaks, I_p^d/I_p^{ind}, depended on the surface coverage of nano-NiO*x*. Nickel oxide (in the NiOOH phase) is believed to mediate the oxidation scheme of FA in such a way that facilitate the charge transfer and/or remove the poisoning CO. On the other hand, modified Au and GC electrodes did not show any significant activity toward FA oxidation.

References

1. S. Zhang, Y. Shao, G. Yin, and Y. Lin, *J. Power Sources*, **195**(4), 1103 (2010).
2. S. Wang, N. Kristian, S. Jiang, and X. Wang, *Electrochem. Commun.*, **10**(7), 961 (2008).
3. M. D. Obradovic, A. V. Tripkovic, and S. L. Gojkovic, *Electrochim. Acta*, **55**(1), 204 (2009).
4. X. Li and I. M. Hsing, *Electrochim. Acta*, **51**(17), 3477 (2006).
5. H. A. Gasteiger, N. M. Markovic, P. N. Ross Jr., and E. J. Cairns, *Electrochim. Acta*, **39**(11), 1825 (1994).
6. M. S. El-Deab, *J. Advanced Research*, **1**, 87 (2010).
7. Y. Wang, X. Wu, B. Wu, and Y. Gao, *J. Power Sources*, **189**(2), 1020 (2009).
8. G. Zhang, Y. Wang, X. Wang, Y. Chen, Y. Zhou, Y. Tang, L. Lu, J. Bao, and T. Lu, *Appl. Catal. B: Environ.*, **102**(4), 614 (2011).
9. J. Wang, P. Holt-Hindle, D. Macdonald, and D. F. Thomas, *Electrochim. Acta*, **53**(23), 6944 (2008).
10. C. Houtman and M. A. Barteau, *Surf. Science*, **248**(2), 57 (1991).
11. X. Yu and P. Pickup, *Electrochim. Acta*, **55**(24), 7354 (2010).
12. A. V. Tripkovic, K. D. Popovic, R. M. Stevanovic, R. Socha, and A. Kowal, *Electrochem. Commun.*, **8**, 1492 (2006).
13. G. Orozco and C. Gutiérrez, *J. Electroanal. Chem.*, **484**, 64 (2000).
14. W. Zhou, J. Xu, Y. Du, and P. Yang, *Int. J. Hydrogen Energy*, **36**(3), 1903 (2011).
15. R. Schrebler, M. A. Del Valle, H. Gómez, C. Veas, and R. Córdova, *J. Electroanal. Chem.*, **380**, 219 (1995).
16. W. Liu and J. Huang, *J. Power Sources*, **189**(2), 1012 (2009).
17. H. Miyake, T. Okada, G. Samjeske, and M. Osawa, *Phys. Chem. Chem. Phys.*, **10**(25), 3662 (2008).
18. Y. Chen, Y. Zhou, Y. Tang, and T. Lu, *J. Power Sources*, **195**(13), 4129 (2010).
19. G. Samjeské, A. Miki, S. Ye, and M. Osawa, *J. Phy. Chem. B*, **110**(33), 16559 (2006).
20. M. S. El-Deab, L. A. Kibler, and D. M. Kolb, *Electrochem. Commun.*, **11**(4), 776 (2009).
21. A. Miki, S. Ye, T. Senzaki, and M. Osawa, *J. Electroanal. Chem.*, **563**, 23 (2004).
22. S. Trasatti and O. A. Petrii, *Pure Appl. Chem.*, **63**(5), 711 (1991).
23. D. Giovanelli, N. S. Lawrence, L. Jiang, T. G. Jones, and R. G. Compton, *Sensors and Actuators B: Chemical*, **88**(3), 320 (2003).
24. A. B. Moghaddam, M. R. Ganjali, R. Dinarvand, T. Razavi, A. Saboury, A. Moosavi, and P. Norouzi, *J. Electroanal. Chem.*, **614**, 83 (2008).
25. M. Pourbaix, *Equilibria in Aqueous Solutions*, p. 286, Pergamon Press, Oxford (1996).
26. Z. Ezerskis and Z. Jusys, *Pure Appl. Chem.*, **73**(12), 1929 (2001).
27. A. Fundo and L. Abrantes, *J. Electroanal. Chem.*, **600**, 63 (2007).
28. I. M. Sadiek, A. M. Mohammad, M. E. El-Shakre, and M. S. El-Deab, *Int. J. Hydrogen Energy*, **37**, 68 (2012).
29. M. Osawa, *Electrocatalytic Reactions on Platinum Electrodes Studied by Dynamic Surface-Enhanced Infrared Absorption Spectroscopy (SEIRAS)*. In *In-situ Spectroscopic Studies of Adsorption at the Electrode and Electrocatalysis*, p. 209, A. Wieckowski, Ed. Elsevier Science BV, Amsterdam (2007).
30. Z. Lijuan, T. Ruili, H. Pu, M. Yuru, and X. Dingguo, *Rare Metal Mat. Eng.*, **39**(6), 945 (2010).
31. M. Arenz, V. Stamenkovic, T. J. Schmidt, K. Wandelt, P. N. Ross, and N. M. Markovic, *Phys. Chem. Chem. Phys.*, **5**(19), 4242 (2003).
32. M. S. El-Deab, L. A. Kibler, and D. M. Kolb *Electrocatal.*, **2**, 220 (2011); M. S. El-Deab, *J. Advanced Research*, **3**, 65 (2012).
33. H. Miyake, T. Okada, G. Samjeské, and M. Osawa, *Phys. Chem. Chem. Phys.*, **10**(25), 3662 (2008).
34. M. A. Barteau, *Catal. Lett.*, **8**(4), 175 (1991).
35. A. M. Fundo and L. M. Abrantes, *Russ. J. Electrochem.*, **42**, 1291 (2006).
36. M. F. Kibria and M. S. Mridha, *Int. J. Hydrogen Energy*, **21**, 179 (1996).
37. L. Vracar and B. E. Conway, *Electrochimica Acta*, **35**, 1919 (1990).
38. P. Rasiyah, A. Tseung, and D. Hibber, *J. Electrochem. Soc.*, **129**, 1724 (1982).